Ignition Catalyzed by Unsupported Metal Nanoparticles

Xiaofei Ma, Lu Liu, Natan Aronhime, and Michael R. Zachariah*

Department of Mechanical Engineering and Department of Chemistry and Biochemistry, University of Maryland, College Park, Maryland 20742, United States

ABSTRACT: The short residence times available in supersonic combustion require some pre-reaction under mixing-controlled-rich conditions and/or methods to lower the reaction temperature for auto-ignition. Adding catalysts could be such an option to achieve this objective. Catalytic ignition of toluene over the surfaces of *in situ*-generated free metal (Fe and Ni) nanoparticles was investigated experimentally in an aerosol reactor. The metal nanoparticles (Fe and Ni) were generated by decomposition of the corresponding metal carbonyls. Gas-phase (aerosol) size distributions along with transmission electron microscopy used to characterize the morphology of catalyst particles at different temperatures are presented. The effluent gas product and the fuel ignition temperature were determined by mass spectrometry. In comparison to non-catalytic homogeneous ignition, the addition of metal nanoparticles can lower the ignition temperature by as much as 150 °C under rich conditions but had little effect under lean conditions. Iron was found to be a more active catalyst than nickel. Inspection of the catalyst product indicated that sintering was occurring at relatively low temperatures presumably as a result of the exothermic reaction on the particle surface. Turnover frequency as high as 80 s^{-1} was achieved, implying a greater catalyst efficiency than commonly found for substrate-stabilized catalysts.

1. INTRODUCTION

Supersonic combustion has received considerable attention recently because of its potential application to hypersonic propulsion systems,[1] such as scramjet engines. These engines operate by supersonic combustion of fuel and atmospheric oxygen. As such, mixing of the fuel and oxidizer is a major constraint because only a very short contact time is available. It is well-known that, under thermal load, the fuel undergoes thermal "cracking" or pyrolysis, leading to the formation of a fuel mixture rich in light hydrocarbons and hydrogen. Ideally, one would like to obtain a pre-reaction under mixing-controlled-rich conditions and/or lower the reaction temperature for auto-ignition. Adding catalysts could be an option to achieve this objective.

Catalysts are often prepared in nanometer-sized particles, so that the total surface area exposed to the reactants is maximized. To preserve the high degree of dispersion and to provide a suitable form of packing for catalyst nanoparticles (NPs), supports on larger and inert materials, such as alumina, silica, titania, and carbon, are usually needed. Most investigations on catalytic reactions are performed with such catalysis configurations. However, in applications where mass-transfer limitations would hinder the combustion rate, boundary layer catalytic limitation provides little advantage. In applications such as for supersonic combustion, monolith supports would never allow for sufficient flows needed. Rather one would prefer to have a free dispersion of catalyst materials that are intimately mixed with the reactant. Furthermore, unsupported (free) NPs eliminate the influence of and the need for support materials. Some aspects of this have already been considered by others. For example, Glikin et al.[2,3] have studied the oxidation of acetic acid over a free iron oxide catalyst. Weber et al.[4,5] investigated the catalytic activity of gas-borne Ni NPs for methanation and concluded that the particle morphology could influence the catalytic performance.

Recently, Shimizu et al.[1] reported work of catalytic methane ignition over the surfaces of freely suspended and *in situ*-generated palladium NPs. In comparison to homogeneous ignition, catalysis by free palladium particles reduced the ignition temperature ~150 K at an equivalence ratio $\Phi \sim 0.5$. In their work, no significant particle size or structure changes were found below and above the ignition temperature. In a later work, Van Devener et al.[6] employed various tools to characterize the composition, structure, and surface chemical state of the *in situ*-generated Pd/PdO catalyst particles during the ignition process. Their results implied that particles must become oxidized before catalytic ignition can be expected. Ignition is important with regard to exothermic decomposition. Wolfe[7] studied the catalytic effect of different metal surfaces for hydrazine decomposition and found that metals with incomplete d orbitals had a catalytic effect in hydrazine decomposition ignition. It is believed that bonding between the N atoms in hydrazine and the incomplete d orbitals of the metal is important. This bonding can initiate hydrazine dissociation and subsequent decomposition and heat release. Our previous work has shown that free (unsupported) metal NPs can lower the decomposition temperature of various liquid fuels under anaerobic conditions.[8]

It is also well-known that metal oxides serve as very active catalysts. For example, PdO is more catalytically active than Pd in methane ignition,[9] and reactivity of PtO$_2$ for CO oxidation is higher than that of a Pt metal surface.[10,11] Under O$_2$-rich conditions, the Ru catalyst surface first oxidizes to form RuO$_2$ before the catalytic reaction takes place.[12] Iron oxide NPs are also attractive catalysts in CO oxidation,[13] catalytic ozonation,[14] and oxidative cracking of heavy petroleum residual oil.[15]
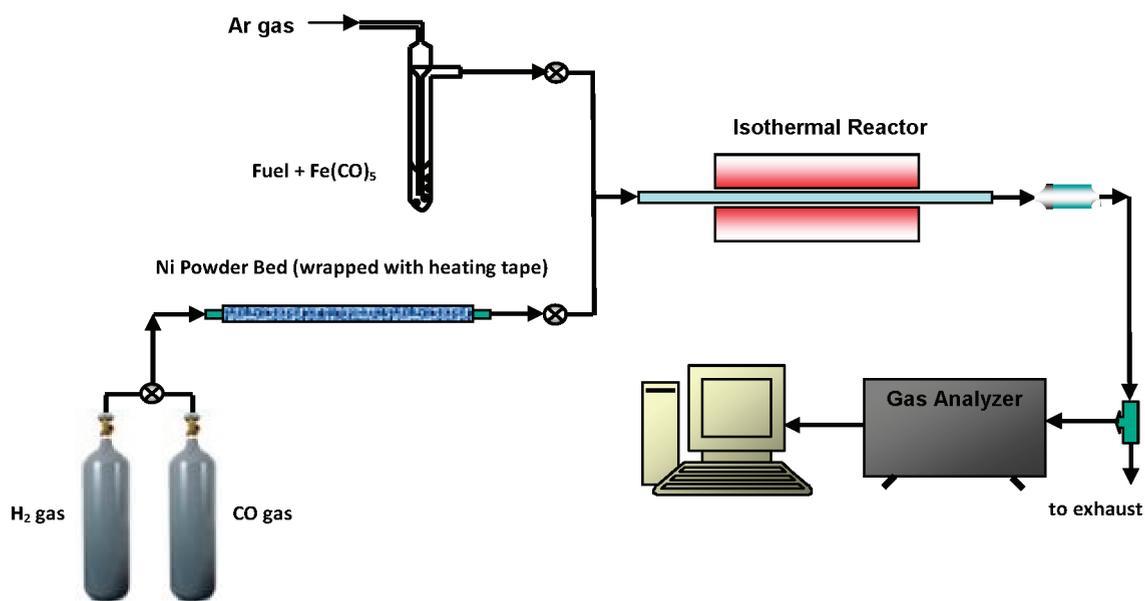
Figure 1. Schematic of the experimental setup for liquid fuel ignition.

Figure 2. TEM image of Fe aggregates.

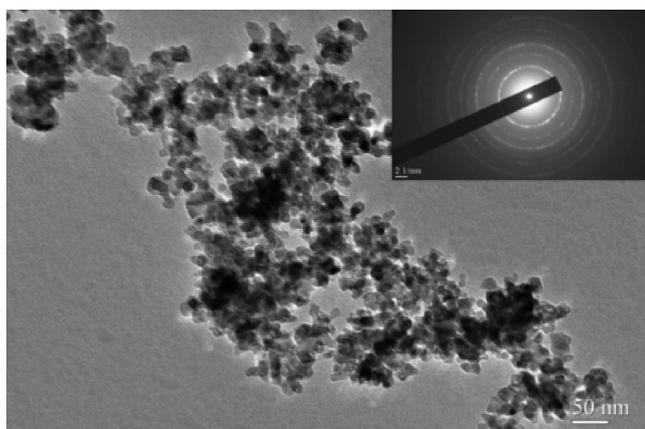**Figure 3.** Particle size distribution of iron NP aggregates generated by iron carbonyl decomposition at 150 °C with different iron precursor concentrations.

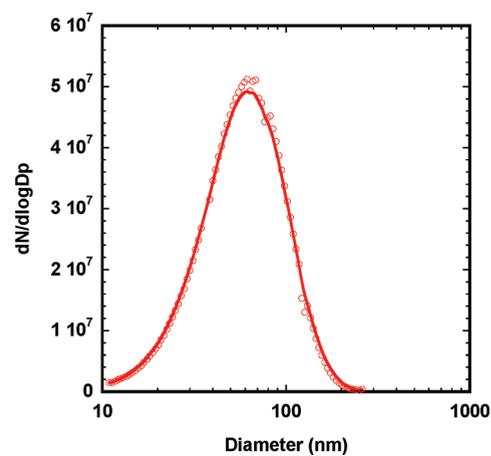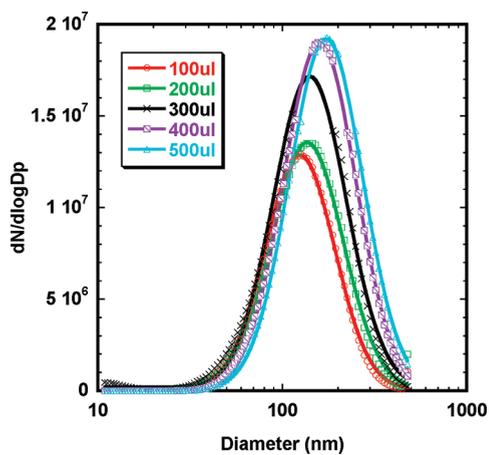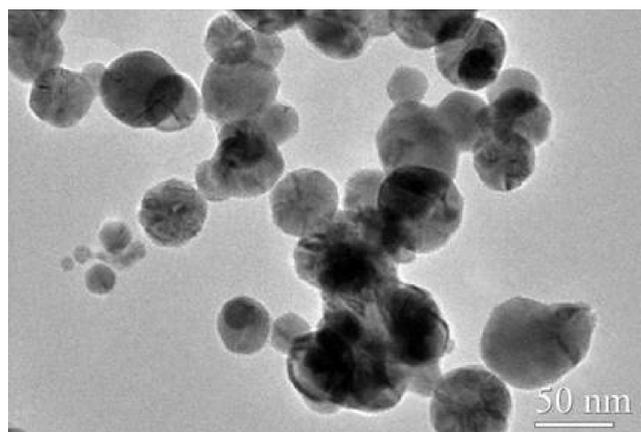**Figure 4.** Particle size distribution of Ni NPs generated by nickel tetracarbonyl decomposition at 450 °C.
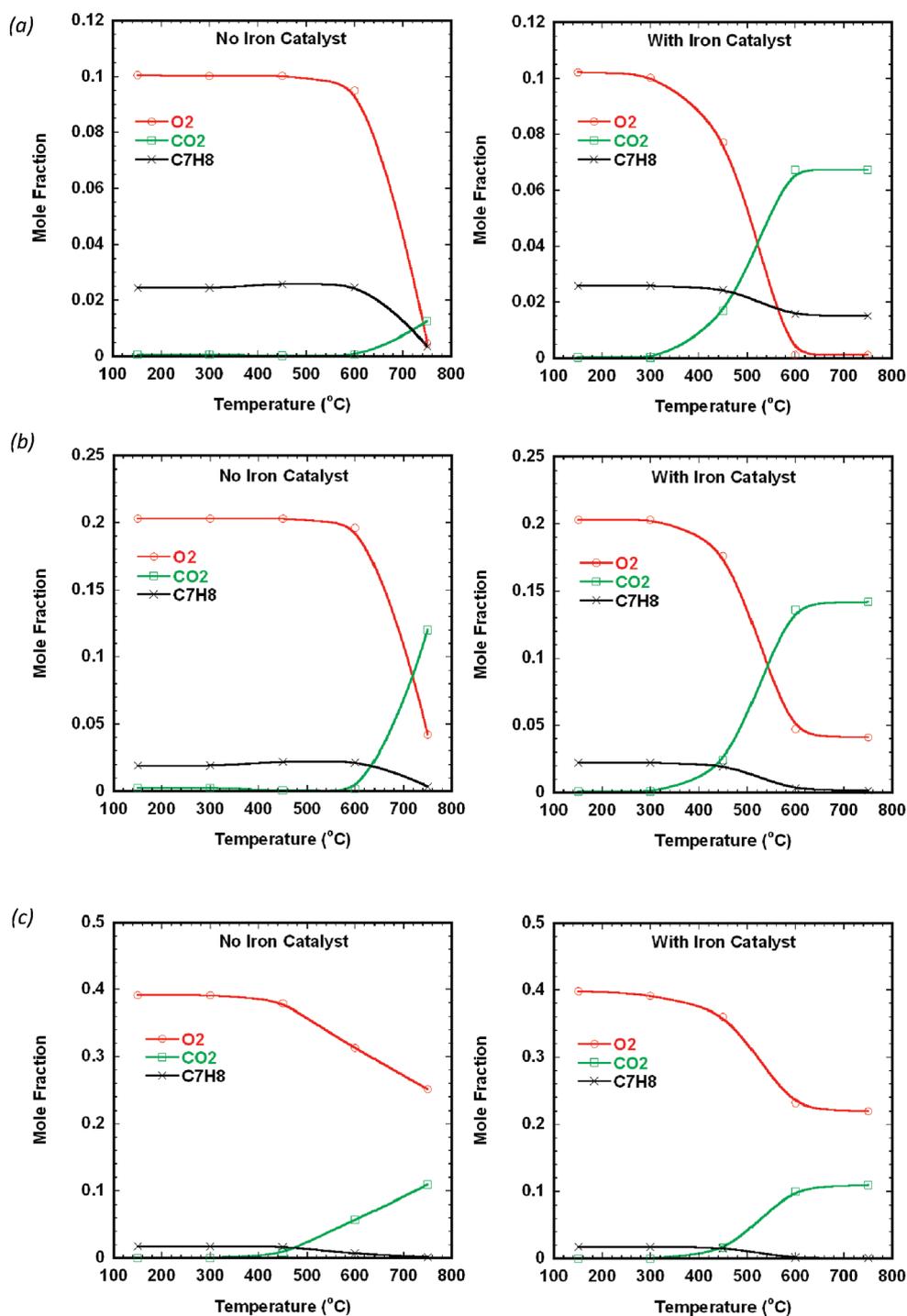

Figure 5. TEM images of Ni NPs.

Figure 6. Mole fraction of fuel (toluene), oxidizer (O_2), and products (CO_2) for a fuel/oxidizer equivalence ratio of (a) 2.3, (b) 1.0, and (c) 0.4.

For any practical application, aromatic compounds must be considered because they can contain up to a third volume percent.[16] Because aromatics are more thermally stable to both pyrolytic and oxidative attack, they would have the most to gain from any enhancement of ignition by catalytic action. Toluene is one of the most important aromatic constituents and is usually employed for many surrogate gasoline, diesel, and jet fuel studies.[17−20] However, toluene exhibits poor ignition properties. In this work, *in situ*-generated unsupported (free) iron and nickel

NPs were used to catalyze the ignition of toluene. The results show that the addition of catalyst NPs (Fe and Ni) can lower the ignition temperature of toluene by about 150 °C at an equivalence ratio of 2.3. With this approach, the catalyst is a one time use, and thus, poisoning is not so great a concern. As such, we can drive the chemistry harder. However, this approach necessarily requires that the catalyst material be inexpensive and the use of precious metals or complex mixtures would not be considered practical.
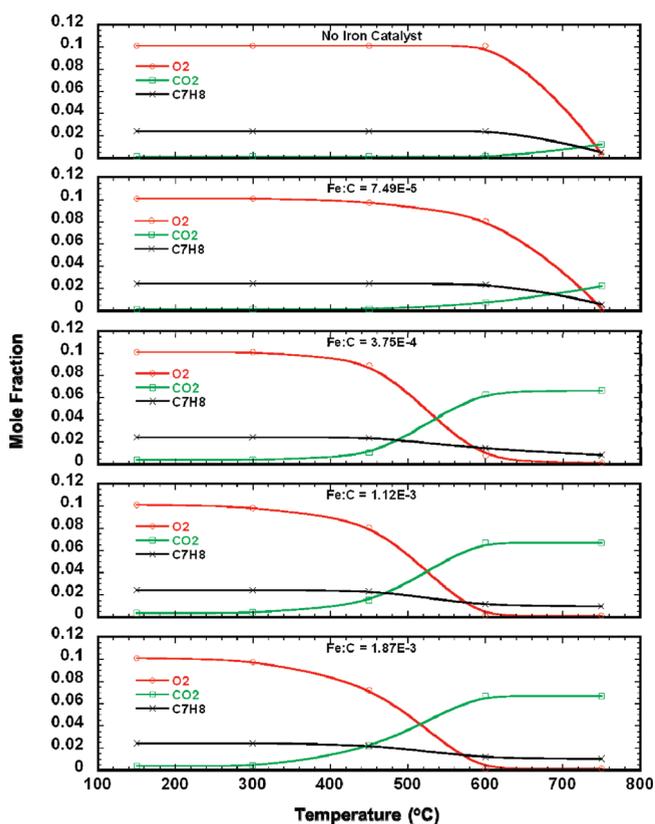
Figure 7. Mole fraction of toluene, CO_2, and O_2 for experiments of different Fe catalyst loading at an equivalence of 2.3.

2. EXPERIMENTAL SECTION

The catalytic ignition of liquid fuels was performed in an aerosol reactor with a controlled gas flow system. The catalytic effects of two aerosol phase catalysts (Fe and Ni NPs) were investigated in this study. A schematic of the experimental setup is presented in Figure 1. The gas mixtures were prepared by bubbling liquid fuel and then mixing the fuel vapor with the oxidizer (oxygen). The catalyst particles were generated *in situ* and mixed with the fuel/oxidizer gas mixture before entering the reactor tube. The aerosol reactor consists of a 22 mm inner diameter and 25 mm outer diameter quartz tube within a 30 cm heated length and with a nominal residence time of ∼1 min. In our experiment, the reactor temperatures were increased at a step of 150 °C. Steady states were achieved at each temperature. Between temperature steps, a heating rate of about 30 °C/min was used.

2.1. *In Situ* Generation of Iron Catalyst Particles. Iron catalyst particles were generated on-the-fly by thermal decomposition of the fuel-soluble iron pentacarbonyl. Iron carbonyl was directly mixed with the liquid fuel, and then the mixture was bubbled and carried by Ar flow to the reactor. The vapor composition is determined by the molar ratio of the two components according to Raoult's law.

2.2. *In Situ* Generation of Nickel Catalyst Particles. The Ni NPs were prepared using gas-phase thermal pyrolysis of nickel tetracarbonyl. Because of the high toxicity of nickel carbonyl, it was generated *in situ* by flowing of a small amount of carbon monoxide through a nickel powder bed. Before each experiment, the nickel bed was heated to ∼350 °C with a hydrogen flow for about 4 h to clean the surface of the nickel powder. After the hydrogen pretreatment, activated nickel powder is reacted with CO at 60 °C to generate $Ni(CO)_4$. Generated $Ni(CO)_4$ was mixed with a flow of Ar and passed to the cracking reactor held at ∼450 °C to generate nickel particles. Because of the low

activation energy of the $Ni(CO)_4$ formation reaction, increases in the Ni bed temperature has little effect on the Ni particle concentration.

2.3. Product Characterization. The size distributions of catalyst particles were measured at the reactor exit using a scanning mobility particle sizer (TSI SMPS), which is composed of an electrostatic classifier (model 3080) and a condensation particle counter (model 3775). A flow rate of 0.3 liter per minute (LPM) of the diluted exhaust was sampled in the SMPS system.

The gaseous effluent was characterized by a mass spectrometer (Stanford Research UGA 300) operating with a mass resolution <0.5 atomic mass unit (amu) at 10% of peak height and a detection limit <1 ppm. The fuel ignition behavior was determined by monitoring the fuel, oxygen, and gas product partial pressures. Argon was used as an inert internal standard and to determine the volume change of gaseous reactants and products during the reaction to assign concentrations. Samples for electron microscopic analysis were collected by electrostatically precipitating the aerosol onto a transmission electron microscopy (TEM) grid using an electrostatic precipitator.

3. RESULTS AND DISCUSSION

3.1. Iron NPs. Figure 2 shows a TEM image of Fe NPs collected at a temperature of 150 °C under an oxygen-free environment with 400 μL of $Fe(CO)_5$ dissolved in 15 mL of toluene. Under this condition, the atomic Fe/toluene molecule ratio was determined to be 0.02. As we can see from the image, the Fe NPs form aggregates, which are composed of small primary particles of sizes between 20 and 30 nm. Figure 3 presents the particle size distribution of iron aggregates generated at 150 °C with different iron carbonyl loadings. The size distributions were measured at the reactor exit using a scanning mobility particle sizer. As shown in the figure, all of the particle size distributions roughly follow a log-normal distribution. The Fe aggregate mobility diameters range from 120 to 170 nm depending upon the loading of the iron precursor. The particle concentration increased with iron pentacarbonyl loading.

3.2. Nickel NPs. Figure 4 presents the particle size distribution of Ni NPs generated by nickel tetracarbonyl decomposition at 450 °C measured by the SMPS system. As we can see from the graph, the particle size distribution peaks at about 60 nm, which is much smaller than the size of Fe aggregates. This is consistent with the particle morphology observed from TEM analysis (Figure 5). As shown in the figure, Ni NPs are less aggregated than Fe NPs. However, because the synthesis temperatures are much higher than that used for the iron case, the Ni primary particle is about 50 nm and, thus, larger than the Fe primary particles.

3.3. Toluene Ignition Catalyzed by Fe NPs. The toluene ignition experiments were conducted at various equivalence ratios. The results for equivalence ratios of 2.3, 1.0, and 0.4 are presented in Figure 6. The partial pressure of each gas species were monitored using a mass spectrometer (SRS UGA 300). A sudden increase in product CO_2 and CO together with the decrease of toluene and O_2 indicated an ignition event. The Fe catalyst loading (Fe/C ratio) in this experiment is estimated to be ∼0.003. As we can see from the plots, for an equivalence ratio of 2.3, the major CO_2 increase and O_2 decrease take place at 750 and 600 °C for non-catalytic and catalytic ignition, respectively, indicating a clear catalytic effect in lowering the ignition temperature. For the catalytic case, in addition to the major ignition event, a smaller O_2 decrease was found at temperatures as low as 450 °C accompanied by an increase in the CO_2 signal.
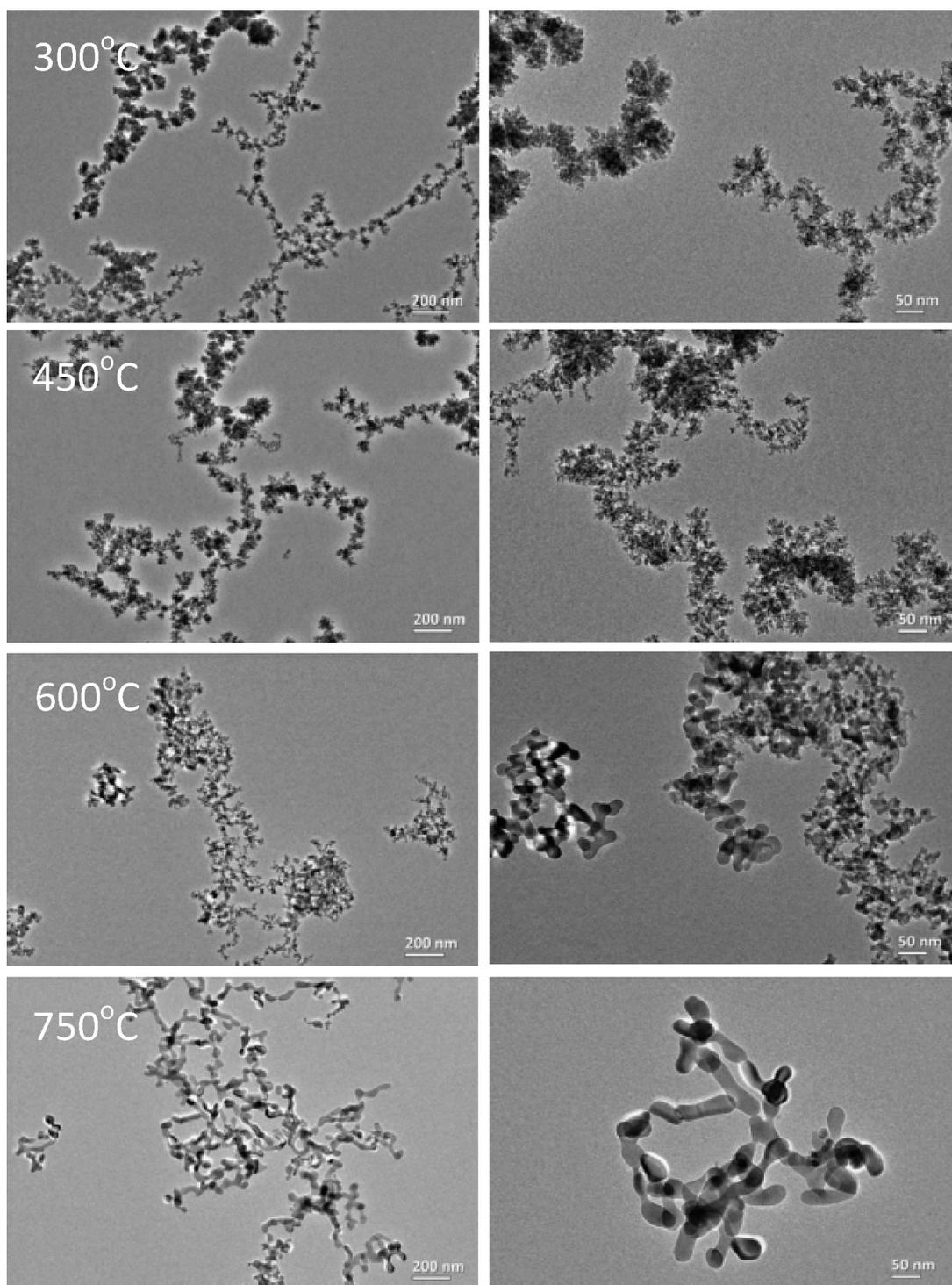
Figure 8. TEM images of Fe NPs at different reactor temperatures.

Similar trends were observed for an equivalence ratio of 1.0. However, for an equivalence ratio of 0.4, no significant changes were observed in toluene ignition behavior. The ignition temperatures for both catalytic and non-catalytic cases were around 600 °C. However, the extent and reaction rate are clearly altered by the catalysts, as can be seen from Figure 6c. With the addition of iron, more toluene and oxygen are consumed and more CO_2 is produced at 600 °C.

The effect of Fe catalyst loading on the ignition temperature of toluene was investigated at a fuel/oxidizer equivalence of 2.3 by varying the $Fe(CO)_5$ concentration in toluene and is shown in Figure 7. Without the Fe catalyst, the ignition temperature of toluene is 750 °C. For a Fe/C ratio of 7.5×10^{-5}, we observe a small increase in CO_2 with a small decrease in O_2 and toluene at 600 °C. However, the major O_2 decrease is still at 750 °C, i.e., at the non-catalytic ignition temperature. As we increase the Fe/C

ratio to the order of $\sim 10^{-4}$, the majority of the O_2 decrease and CO_2 increase occurs at 600 °C and the ignition temperature decreased to ~ 600 °C. However, a further increase in the Fe loading shows no effect in either the ignition temperature or the CO_2 or O_2 conversion rate. In comparison to the non-catalytic case, the CO_2 mole fraction in the catalytic case increases more than 4 times at the temperature of 750 °C, which indicated that the catalyst also promotes CO to CO_2 conversion. On the basis of the catalyst loading (Fe/C ratio of 3.75×10^{-4}), toluene conversion of 65%, and the primary particle size of the catalyst particles and assuming that only surface atoms can contribute to the chemistry, we can estimate the catalyst turnover number, TON = moles of reactant converted per moles of catalyst surface atoms available. Assuming a primary particle size of ~ 30 nm, we find a TON ~ 4900. Then, on the basis of our nominal residence time of ~ 1 min, we can estimate the catalyst turnover frequency, TOF ~ 80 s^{-1}. This compares very favorably to the reported TOF for supported iron/iron complex catalysts in hydrocarbon oxidation, which usually have TOF values <10 s^{-1}.[21-25] This latter point is not surprising given the decreased mass-transfer resistance that free floating catalysts should provide.

Inspection of the catalyst product indicated that considerable changes were occurring to the particles during the course of the chemistry. Particles were collected for TEM characterization at
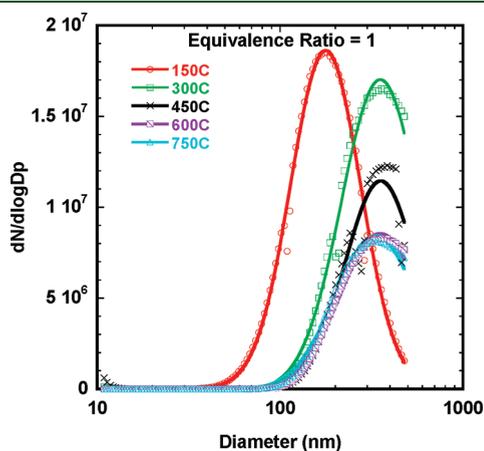
different reactor temperatures at an equivalence ratio of 1.0 and are presented in Figure 8. Particles at 300 °C (Figure 8) exhibit a flower-shaped morphology with small oxide branches growing from each primary particle, indicating partial oxidation of the Fe particles. A similar morphology was observed at 450 °C. As the reactor temperature increased to 600 °C (the ignition temperature from Figure 6b), particle sintering can be observed. The partially melted particle surface indicates high local temperatures, resulting from an exothermic oxidation reaction. As the reactor temperature increased to 750 °C, more sintering is observed. The reader is reminded that the bulk melting temperatures for both iron and iron oxide are above 1500 °C.

A series of particle size distributions of catalyst Fe particles were also measured at the exit of the reactor under different reactor temperatures. The equivalence ratio was kept at 1.0 during the measurement. The results presented in Figure 9 show that a large increase in aggregate size occurs at 300 °C with the particle mobility size doubling from that at 150 °C. The large size increase is due to more complete iron carbonyl decomposition and Fe particle partial oxidation at 300 °C. This is consistent with the small oxygen concentration decrease at 300 °C. A further increase in the reactor temperature leads to a slightly smaller particle peak size accompanied by lower particle concentrations. The smaller particle size at a higher temperature is consistent with the sintering of particles, while a lower particle concentration is due to the increased diffusional particle loss at high temperatures.

3.4. Toluene Ignition Catalyzed by Ni NPs. The experiments of toluene ignition catalyzed by Ni NPs were carried out under various equivalence ratios. Because Ni NPs were generated by flowing CO through a Ni powder bed in the catalytic ignition experiment, a small CO flow was also added in the non-catalytic experiment, such that the total flow rate was the same for both cases. Figure 10 shows the comparable results for toluene ignition with an equivalence ratio of 4.6. Two observations stand out. First, adding Ni NPs lowers the ignition temperature of toluene by about 150 °C. Second, more CO_2 was produced in the catalytic experiment as a result of more complete oxidation. Similar results were also observed in the Fe catalytic experiments. The ignition experiments were also carried out at equivalence ratios of 2.3, 1.0, and 0.8. For the non-catalytic experiments, as the equivalence ratios decrease, the autoignition temperature
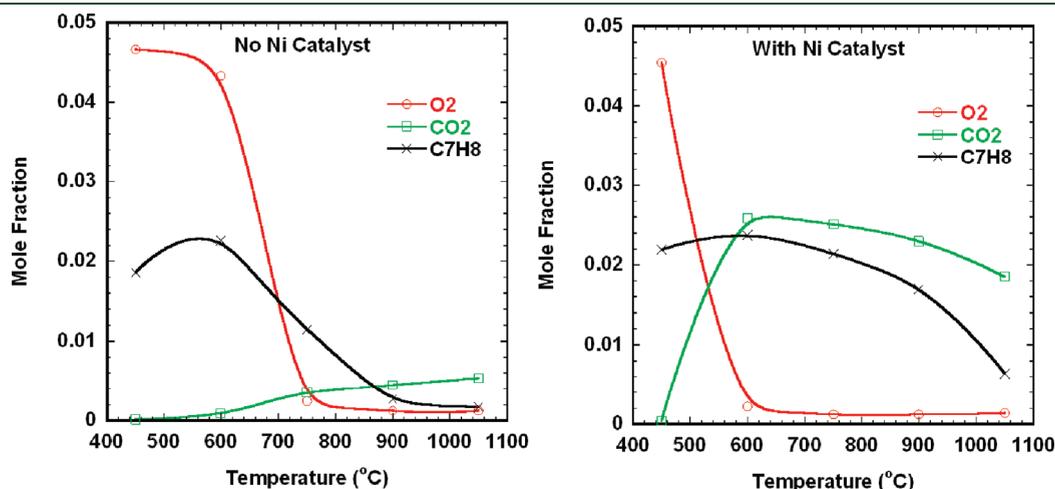

Figure 9. Particle size distributions of Fe NPs at different temperatures.

Figure 10. Toluene ignition catalyzed by Ni NPs.

also decreases. For lower equivalence ratios (below 1.0), adding Ni NP catalysts did not change the ignition behavior of the fuel, similar to that observed in the Fe experiments. Given that the Ni catalyst loading (Ni/C ratio) in this experiment is estimated to be ~0.05, which is about 16 times more than that of Fe, and considering that the specific surface area of Fe particles is about 4 times larger than that of Ni, the Ni catalyst particles are still not as effective as Fe particles.

Unlike the case of iron particles, Ni did not show significant restructuring and/or sintering effects. The TEM image in
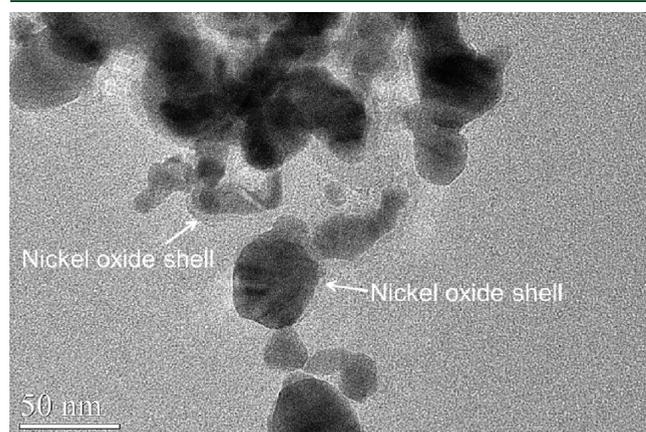

Figure 11. TEM image of Ni catalyst particles reacted at 750 °C.

Figure 11 of Ni catalyst particles collected after the reaction at 750 °C shows the appearance of an oxide shell, which could not be observed as easily in the much smaller iron particles.

3.5. Mechanism of Catalytic Ignition. As shown in Figure 8, the Fe NPs undergo structural transformation (sintering) at the fuel ignition temperature. This sintering effect is likely initiated by the rapid heat release from the Fe NP oxidation process. Thus, the Fe oxidation kinetics must play a critical role in the catalytic ignition process. This metal NP oxidation-induced catalytic ignition effect is consistent with previous methane ignition studies using Pd NP catalysts.[1,6] Actually, iron oxide NPs are active catalysts in CO and methane oxidation. In CO oxidation,[13] iron oxide NPs act as both a catalyst and an oxidant. In our experiment, the catalytic effects are more significant under rich rather than lean cases. Keep in mind that, even under very rich conditions, there is sufficient gas-phase oxygen to oxidize the particles. Thus, under both rich and lean conditions, the presumed catalyst surface should be an oxide. It would appear then that, under lean conditions, the autoignition temperature is low enough that the catalytic effect is minor.

In the catalytic process, the fuel molecules react with lattice oxygen in iron oxide and active oxygen species in the reacting flow.[26] To further explore the effect of NPs on toluene ignition, mass spectra of the reaction products were collected at each reaction temperature. The major detectable reaction products were hydrogen, carbon dioxide, carbon monoxide, methane, ethylene, acetylene, and benzene. The concentration variations with the temperature for the selected reactant and products are
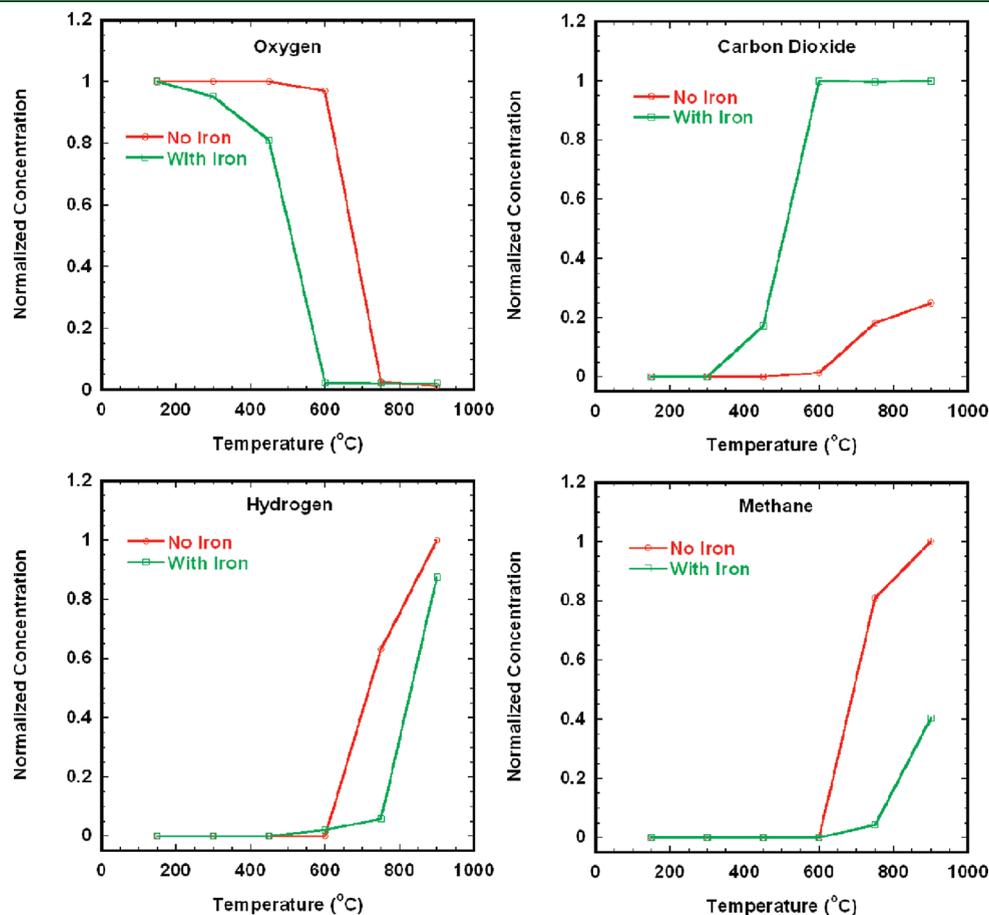

Figure 12. Concentrations of selected gas species.

presented in Figure 12. Several trends can be observed from the plots. With the addition of iron catalysts, the oxygen concentration starts to decrease at a much lower temperature than the non-catalytic case. Correspondingly, the product carbon dioxide concentration starts to increase at a lower temperature and saturated at about 600 °C. The saturation concentration of carbon dioxide in the catalytic case is also much higher. The overall methane concentration is higher in the non-catalytic case. Hydrogen was detected at 600 °C in the catalytic case, while in the non-catalytic case, hydrogen was detected at 750 °C.

The detailed toluene oxidation mechanism is very complex, but it is generally believed that the initiation of toluene oxidation is the pyrolytic cleavage of a hydrogen atom from the methyl side chain at high temperatures and the O_2 abstraction of a H from the side chain at low temperatures.[7] The products of the initiation step then undergo a series of chemical transformations to form smaller intermediates. Finally, the smaller intermediate products undergo their own oxidation processes and generate carbon dioxide and water. With the general mechanism of toluene oxidation, we can summarize the effects of catalysts in toluene ignition. As we can see from Figure 12, with the addition of Fe catalysts, oxygen starts to decrease as low as 300 °C, which is consistent with the oxidation of iron NPs. No carbon dioxide was detected. A further decrease in oxygen occurs at 450 °C, which corresponds to the attack of toluene by oxygen molecules. At this temperature, a small amount of carbon dioxide is detected as the reaction product. The lower oxygen attack temperature reflects the enhanced oxidative dissociation effect on the iron oxide NP surfaces. As the temperature increases to 600 °C, hydrogen is detected as a result of high-temperature toluene pyrolysis. The generated H atoms initiate the H_2-O_2 radical pool, which leads to radical attack on toluene, and branching steps, eventually leading to ignition. A much higher carbon dioxide concentration is observed in the catalytic case (about 4 times higher than the non-catalytic case), which suggests a thorough oxidation reaction. Figure 12 shows a lower methane concentration at high temperatures in the catalytic ignition. The detected ethylene and acetylene concentrations (not shown) were also lower in the catalytic case. In summary, the addition of iron catalysts has three effects in catalyzing toluene ignition. First, the iron oxide particles converted from iron catalysts can promote oxygen attack of toluene molecules. Second, the catalyst particles promote the fuel pyrolysis. The similar trend was also observed in our previous studies in catalytic fuel decomposition.[8] Third, the addition of iron catalysts accelerates the oxidation of smaller molecules.

4. CONCLUSION

Catalytic ignition of toluene over *in situ*-generated free metal (Fe and Ni) NPs was investigated in an aerosol reactor. Iron and nickel particles were generated by gas-phase pyrolysis of their corresponding carbonyl. In comparison to non-catalytic homogeneous ignition, the addition of metal NPs can lower the ignition temperature of toluene by as much as 150 °C. A high turnover frequency (TOF ∼ 80 s^{-1}) was found for Fe NPs at an equivalence ratio of 2.3. Electron microscopic analysis shows that the Fe NPs undergo structural transformation (oxidation and sintering), which is likely initiated by the rapid heat release from the Fe NP oxidation process. The similar oxidation process was also observed for Ni catalysts. However, no significant restructuring or sintering effect was found. On the basis of the

mass spectra of the products at different reactor temperatures, we propose that the *in situ*-generated metal oxide NPs (converted from metal NPs) promote the breakdown of fuel molecules as well as the oxidation of small intermediate hydrocarbon products.

■ AUTHOR INFORMATION

Corresponding Author
*E-mail: mrz@umd.edu.

■ ACKNOWLEDGMENT

■ REFERENCES

(1) Shimizu, T.; Abid, A. D.; Poskrebyshev, G.; Wang, H.; Nabity, J.; Engel, J.; Yu, J.; Wickham, D.; Van Devener, B.; Anderson, S. L.; Williams, S. Methane ignition catalyzed by in situ generated palladium nanoparticles. *Combust. Flame* **2009**, *157* (3), 421–435.

(2) Glikin, M.; Kutakova, D.; Prin, E. Unsteady processes and aerosol catalysis. *Chem. Eng. Sci.* **1999**, *54* (20), 4337–4342.

(3) Glikin, M. A. Aerosol catalysis. *Theor. Found. Chem. Eng.* **1996**, *30* (4), 390–394.

(4) Weber, A. P.; Seipenbusch, M.; Binnig, J.; Kasper, G. Influence of the particle morphology on the activity of nanometer platinum aerosol catalysts. *Part. Part. Syst. Charact.* **2002**, *19* (5), 300–305.

(5) Weber, A. P.; Seipenbusch, M.; Kasper, G. Application of aerosol techniques to study the catalytic formation of methane on gasborne nickel nanoparticles. *J. Phys. Chem. A* **2001**, *105* (39), 8958–8963.

(6) Van Devener, B.; Anderson, S. L.; Shimizu, T.; Wang, H.; Nabity, J.; Engel, J.; Yu, J.; Wickham, D.; Williams, S. In situ generation of Pd/PdO nanoparticle methane combustion catalyst: Correlation of particle surface chemistry with ignition. *J. Phys. Chem. C* **2009**, *113* (48), 20632–20639.

(7) Glassman, I.; Yetter, R. A. *Combustion*; Academic Press: New York, 2008.

(8) Ma, X. F.; Lall, A. A.; Aronhime, N.; Zachariah, M. R. Catalytic decomposition of liquid hydrocarbons in an aerosol reactor: A potential solar route to hydrogen production. *Int. J. Hydrogen Energy* **2010**, *35* (14), 7476–7484.

(9) Ciuparu, D.; Lyubovsky, M. R.; Altman, E.; Pfefferle, L. D.; Datye, A. Catalytic combustion of methane over palladium-based catalysts. *Catal. Rev.−Sci. Eng.* **2002**, *44* (4), 593–649.

(10) Hendriksen, B. L. M.; Frenken, J. W. M. CO oxidation on Pt(110): Scanning tunneling microscopy inside a high-pressure flow reactor. *Phys. Rev. Lett.* **2002**, *89* (4), No. 046101.

(11) Hendriksen, B. L. M.; Bobaru, S. C.; Frenken, J. W. M. Bistability and oscillations in CO oxidation studied with scanning tunnelling microscopy inside a reactor. *Catal. Today* **2005**, *105* (2), 234–243.

(12) Over, H.; Kim, Y. D.; Seitsonen, A. P.; Wendt, S.; Lundgren, E.; Schmid, M.; Varga, P.; Morgante, A.; Ertl, G. Atomic-scale structure and catalytic reactivity of the $RuO_2(110)$. *Surf. Sci.* **2000**, *287* (5457), 1474–1476.

(13) Li, P.; Miser, D. E.; Rabiei, S.; Yadav, R. T.; Hajaligol, M. R. The removal of carbon monoxide by iron oxide nanoparticles. *Appl. Catal., B* **2003**, *43* (2), 151–162.

(14) Jung, H.; Park, H.; Kim, J.; Lee, J. H.; Hur, H. G.; Myung, N. V.; Choi, H. Preparation of riotic and abiotic iron oxide nanoparticles (IOnPs) and their properties and applications in heterogeneous catalytic oxidation. *Environ. Sci. Technol.* **2007**, *41* (13), 4741–4747.

(15) Funai, S.; Fumoto, E.; Tago, T.; Masuda, T. Recovery of useful lighter fuels from petroleum residual oil by oxidative cracking with steam using iron oxide catalyst. *Chem. Eng. Sci.* **2010**, *65* (1), 60–65.

(16) Shen, H. P. S.; Oehlschlaeger, M. A. The autoignition of C_8H_{10} aromatics at moderate temperatures and elevated pressures. *Combust. Flame* **2009**, *156* (5), 1053–1062.

(17) Edwards, T.; Maurice, L. Q. Surrogate mixtures to represent complex aviation and rocket fuels. *J. Propul. Power* **2001**, *17* (2), 461–466.

(18) Violi, A.; Yan, S.; Eddings, E. G.; Sarofim, F.; Granata, S.; Faravelli, T.; Ranzi, E. Experimental formulation and kinetic model for JP-8 surrogate mixtures. *Combust. Sci. Technol.* **2002**, *174* (11–2), 399–417.

(19) Eddings, E. G.; Yan, S. H.; Ciro, W.; Sarofim, A. F. Formulation of a surrogate for the simulation of jet fuel pool fires. *Combust. Sci. Technol.* **2005**, *177* (4), 715–739.

(20) Humer, S.; Frassoldati, A.; Granata, S.; Faravelli, T.; Ranzi, E.; Seiser, R.; Seshadri, K. Experimental and kinetic modeling study of combustion of JP-8, its surrogates and reference components in laminar nonpremixed flows. *Proc. Combust. Inst.* **2007**, *31*, 393–400.

(21) Huang, G.; Guo, Y. A.; Zhou, H.; Zhao, S. K.; Liu, S. Y.; Wang, A. P.; Wei, J. F. Oxidation of cyclohexane with a new catalyst $(TPPFe^{III})_2O$ supported on chitosan. *J. Mol. Catal. A: Chem.* **2007**, *273* (1–2), 144–148.

(22) Isci, U.; Afanasiev, P.; Millet, J. M. M.; Kudrik, E. V.; Ahsen, V.; Sorokin, A. B. Preparation and characterization of mu-nitrido diiron phthalocyanines with electron-withdrawing substituents: Application for catalytic aromatic oxidation. *Dalton Trans.* **2009**, *36*, 7410–7420.

(23) Jia, J. F.; Pillai, K. S.; Sachtler, W. M. H. One-step oxidation of benzene to phenol with nitrous oxide over Fe/MFI catalysts. *J. Catal.* **2004**, *221* (1), 119–126.

(24) Guo, C. C.; Chu, M. F.; Liu, Q.; Liu, Y.; Guo, D. C.; Liu, X. Q. Effective catalysis of simple metalloporphyrins for cyclohexane oxidation with air in the absence of additives and solvents. *Appl. Catal., A* **2003**, *246* (2), 303–309.

(25) Schuchardt, U.; Pereira, R.; Rufo, M. Iron(III) and copper(II) catalysed cyclohexane oxidation by molecular oxygen in the presence of *tert*-butyl hydroperoxide. *J. Mol. Catal. A: Chem.* **1998**, *135* (3), 257–262.

(26) Fumoto, E.; Matsumura, A.; Sato, S.; Takanohashi, T. Kinetic model for catalytic cracking of heavy oil with a zirconia–alumina–iron oxide catalyst in a steam atmosphere. *Energy Fuels* **2009**, *23*, 5308–5311.